Journal of Sound and Vibration (1998) **214**(2), 359–375
Article No. sv981582

NON-LINEAR VIBRATIONS OF A SPHERE–PLANE CONTACT EXCITED BY A NORMAL LOAD

J. Sabot, P. Krempf and C. Janolin

Laboratoire de Tribologie et Dynamique des Systèmes, *CNRS*, *UMR* 5513,
Ecole Centrale de Lyon, *F*-69131 *Ecully Cedex*, *France*

(*Received* 24 *June* 1996, *and in final form* 2 *March* 1998)

Many mechanisms use Hertzian contacts. During operation, these contacts are generally excited by a dynamic normal load. To study the non-linear vibrations of a sphere–plane contact we have built a device which uses a symmetrical plane–sphere–plane contact. The first step was to study free vibrations under a static normal load. Our elastic system can be summarized as a one-degree-of-freedom non-linear oscillator. Numerical and analytical methods were used to predict the main properties of the dynamic response (contact natural frequency, frequency contents, softening behaviour). A first set of experiments, on free contact vibrations, has shown that the measured contact natural frequency is in very good agreement with the theory, and that in dry contacts the contact damping is small and can be reasonably described by an equivalent viscous damping. In lubricated contacts, a fluid pumping mechanism can add a noticeable amount of damping. A second set of experiments on forced contact vibrations was performed in order to study dynamic contact load during the principal non-linear resonance. A softening dynamic behaviour is observed and the level of the dynamic contact load can be greater than twice the static load just before the jump observed during a scan of decreasing frequency.

1. INTRODUCTION

In many systems such as machines, robots, road, rail, sea or air vehicles, a variety of mechanisms is used to ensure the transformation of movements and stresses generated by motors. These mechanical devices generally use Hertzian contacts. This is the case for ball or roller bearings, gears, push-cam systems, etc. During the operation of the system, the Hertzian contacts are stimulated by normal and tangential loads.

In the specific case of sphere–plane type contacts subject to static loads, it is possible to describe the relative displacement field of both solids in contact, the geometry of the contact area, the distribution of the stresses within this area, as well as the stress field within elastic solids in contact [1–4].

The case of Hertzian contacts stimulated by a purely normal and dynamic load characterized by a harmonic time variation superimposed on an average value (static normal load) constitute a basic case that applies to numerous systems because in hydrodynamic or elastohydrodynamic lubrication mode, the normal load is much higher than the tangential load. Moreover, the operation of the mechanical device generally leads to a variation in the normal load around its average value. For instance, in a gearbox, transmission error leads to a dynamic load on the teeth and on the ball or roller-bearings [5].

Because of the non-linear contact stiffness, the excitation of a Hertzian contact by a harmonic load produces non-linear vibrations. Depending on the value of the harmonic load frequency, non-linear resonance phenomena may occur and cause high amplification

0022–460X/98/270359 + 17 $30.00/0

of the normal stresses applied within the contact area. To ensure the right approach to tribology solutions and a good evaluation of the vibroacoustic response of a mechanical system, these dynamic contact loads should be taken into consideration.

First, the normal vibrations of a cylinder–cylinder contact [6] and a sphere–plane contact [7] were studied. Other works have been carried out to analyze the influence of normal vibrations on the friction factor average value [8, 9]. However, there has not yet been any systematic approach either to describe the dynamic overloads caused by non-linear normal vibrations within a sphere–plane contact, or to provide quantitative information on the various mechanisms which contribute to the dissipation capacity associated with this type of contact vibration.

This theoretical and experimental analysis is aimed at gaining a better understanding of the dynamic response characteristics of a sphere–plane contact excited by a purely normal load equal to the sum of a static load and a harmonic load of low amplitude. For the experimental analysis of the problem, an original device has been designed, built and used.

In section 2, a non-linear elastic model is associated with the system studied so that, once the model has been validated and the little known parameters identified, a global mathematical analysis may be carried out to describe the solution of the non-linear differential equation that governs the vibrations of the system. After describing and testing the major numerical integration methods for this equation, the most efficient method is selected for numerical simulations of the vibration behaviour of the plane–sphere–plane system. Similarly, among the major approximate analytical methods, the multiple scales method is used to provide an approximate solution. A comparison between these analytical results and the previous numerical results then allows the numerical integration method selected to be validated.

The experimental results on the non-linear free vibrations of the system are described in section 3. By analyzing the contact natural frequency, the mathematical model described in section 2 can be validated. Information is then provided relating to the possible choices in the damping function, and the measured damping values in a sphere–plane contact are analyzed.

The experimental results associated with the forced vibrations are described and discussed in section 4. The principal non-linear resonance phenomenon is studied in detail. Important dynamic normal overloads can be observed and the non-linear characteristics of the forced responses are analyzed.

2. MODELLING AND MATHEMATICAL ANALYSIS

2.1. MECHANICAL SYSTEM AND ASSOCIATED MODEL

To analyze the Hertzian sphere–plane contact, the device described in Figure 1 was built. The moving solid is the upper cylinder of mass M. It moves along a vertical axis and compresses the sphere which is placed on the upper plane of a thick disc. The two parallel planes between which the sphere is placed are horizontal.

Under the effect of the cylinder weight and the contact normal stiffness, the upper plane reaches an equilibrium position z_0 and the sphere is prestressed. A vertical harmonic load $F_e \cos(\omega t)$ applied on the cylinder by means of an adequately hung vibrating exciter causes a dynamic displacement $z(t)$ of the cylinder around z_0.

A normal Hertzian stiffness and an *a priori* unknown damping function C are associated with each of the two symmetrical contacts. The two-degree-of-freedom non-linear elastic model associated with the system studied is illustrated in Figure 2(a). If the mass m of the

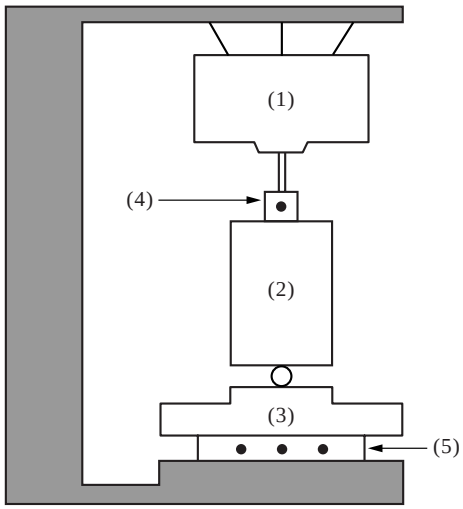

Figure 1. Experimental device: (1) vibration exciter; (2) moving cylinder; (3) fixed plane; (4) impedance head; (5) three components force transducer.

sphere is very small compared with that of the cylinder, it can be easily shown that the previous model can be summarized as a one-degree-of-freedom non-linear oscillator, characterized by a mass M, a new non-linear stiffness equivalent to the two previous Hertzian stiffnesses placed in series and a damping function $C' = 2C$. The differential equation governing the non-linear vibrations of this oscillator can then be given by

$$M\ddot{z} + C'(z, \dot{z})\dot{z} + k'(z_0 + z)^{3/2} = F_s + F_e \cos \omega t, \tag{1}$$

where $F_s = Mg$ is the normal static load (weight of the cylinder) and $k' = 2^{-3/2}k$ is a constant which can be deduced from Hertz's theory of elastic point contact [3]. If materials of the sphere and the plane are identical (Young's modulus E and Poisson ratio v) then

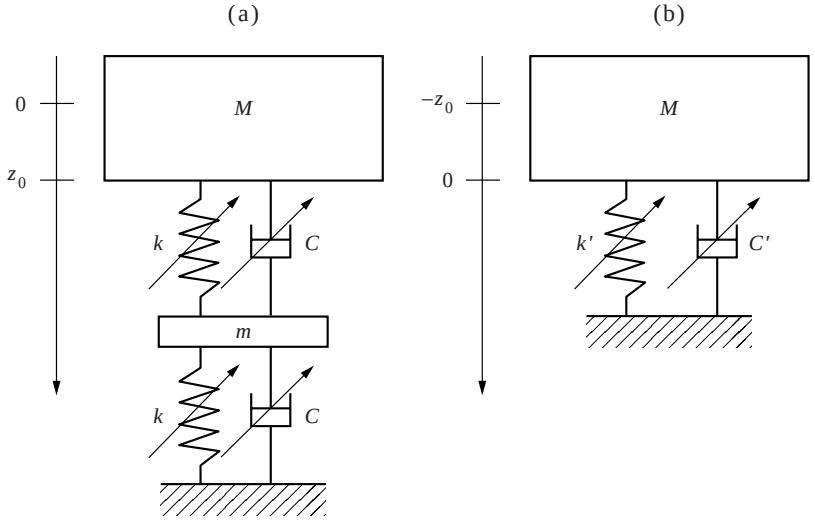

Figure 2. Dynamic models of the experimental device. (a) Two-degree-of-freedom model; (b) one-degree-of-freedom model.

the constant k for a single sphere–plane contact is given by $k = 4E\sqrt{R}/3(1 - v^2)$, where R is the sphere radius.

Equation (1) is valid only if the deformations within the solids in contact remain elastic and if there is no contact loss between sphere and upper plane ($z \geqslant -z_0$).

2.2. DIMENSIONLESS EQUATION

In order to write equation (1) in dimensionless form, one can consider the contact natural frequency ω_N [7]. This frequency is obtained by linearizing the elastic contact force around the static equilibrium position z_0 as

$$k'(z_0 + z)^{3/2} = F_s + (\tfrac{3}{2} k' z_0^{1/2})z, \tag{2}$$

where $(\frac{3}{2} k' z_0^{1/2})$ is the linearized stiffness. Hence, the contact natural frequency is defined by

$$\omega_N^2 = \tfrac{3}{2} z_0^{1/2}(k'/M). \tag{3}$$

Further, one can define a dimensionless time $\tau = \omega_N t$, a dimensionless forced frequency $\bar{\omega} = \omega/\omega_N$, a dimensionless displacement $\eta = \frac{3}{2}(z/z_0)$, a dimensionless external load $\sigma = F_e/F_s$ and a damping ratio $\zeta = C'(z, \dot{z})/2M\omega_N$ to obtain a new equation for the cylinder's motion,

$$\ddot{\eta} + 2\zeta(\eta, \dot{\eta})\dot{\eta} + (1 + \tfrac{2}{3}\eta)^{3/2} = 1 + \sigma \cos \bar{\omega}\tau, \tag{4}$$

which remains valid for $\eta \geqslant -3/2$.

In order to obtain approximate expressions describing the motion by analytical methods [10, 11] one can approach the elastic contact force by expanding it in a third order Taylor series

$$(1 + \tfrac{2}{3}\eta)^{3/2} \cong 1 + \eta + \tfrac{1}{6}\eta^2 - \tfrac{1}{54}\eta^3. \tag{5}$$

2.3. UNDAMPED FREE VIBRATIONS

The undamped free vibrations study can be interesting for analyzing the dynamic behaviour of the forced response. In particular, knowledge of the natural frequency ω_0 versus amplitude of the undamped free response gives information about the frequency response curves of the forced damped motion, because this relation constitutes the backbone of the principal non-linear resonance.

Letting $\sigma = 0$ and $\zeta = 0$ in equation (4) yields the governing equation of the undamped free vibrations of the cylinder:

$$\ddot{\eta} + (1 + \tfrac{2}{3}\eta)^{3/2} = 1. \tag{6}$$

If one wants to find the natural frequency ω_0, one can introduce at $\tau = 0$ the initial conditions

$$\dot{\eta} = 0 \qquad \text{and} \qquad \eta = -\alpha \geqslant -\tfrac{3}{2} \qquad (\text{or } z/z_0 = -\tfrac{2}{3}\alpha). \tag{7}$$

Considering the following normalized Hamiltonian H of the conservative system,

$$H = \tfrac{1}{2}\dot{\eta}^2 + \tfrac{3}{5}(1 + \tfrac{2}{3}\eta)^{5/2} - \eta = H_0, \tag{8}$$

which remains constant and equal to

$$H_0 = \tfrac{3}{5}(1 - \tfrac{2}{3}\alpha)^{5/2} + \alpha, \tag{9}$$

one can obtain the maximum amplitude η_{max} of the free undamped response by solving equation (8) with $\dot{\eta} = 0$.

From equations (8) and (9) one can also express the velocity response as

$$|\dot{\eta}| = \sqrt{2}[H_0 + \eta - \tfrac{3}{5}(1 + \tfrac{2}{3}\eta)^{5/2}]^{1/2}, \tag{10}$$

and finally, the period T_0 of undamped free vibrations can be obtained by numerical integration of the integral

$$\tau_0 = \omega_N T_0 = 2 \int_{-\alpha}^{\eta\, max} \frac{\mathrm{d}\eta}{|\dot{\eta}|}. \tag{11}$$

Results are illustrated in Figure 3. One can observe the softening character of the Hertzian contact non-linearity and the non-symmetrical character of the response related to the non-symmetrical contact stiffness. Comparisons with results obtained by numerical integration of equation (6) have confirmed this behaviour. The numerical integration permits one also to obtain the entire free response of the moving cylinder.

To choose among classical numerical integration schemes [12], four of them have been tested (Newmark-beta, Runge–Kutta, central-difference and Houbolt methods). Finally, they gave results that may be regarded as identical, since for two different method types, the period variation never exceeds 0·02% and the amplitude variation 0·25%. The explicit central differences method proved to be the most efficient in terms of computation time. Implicit methods require the solution of algebraic equations, needing an additional linearization procedure. The computation time is hence longer than for the explicit central differences method. The Runge–Kutta method proved to be the most expensive in terms of computation time, and all the more so as its order is high. The central differences method was therefore selected for the solutions and the numerical simulations of our non-linear dynamic problems.

Finally, classical perturbation methods can also be used to obtain an approximate solution of equation (6) in conjunction with the approximate expression defined in equation (5). Consider the resulting equation of motion,

$$\ddot{\eta} + \eta + a_2 \eta^2 + a_3 \eta^3 = 0, \qquad \text{where} \qquad a_2 = 1/6 \qquad \text{and} \qquad a_3 = -1/54. \tag{12}$$

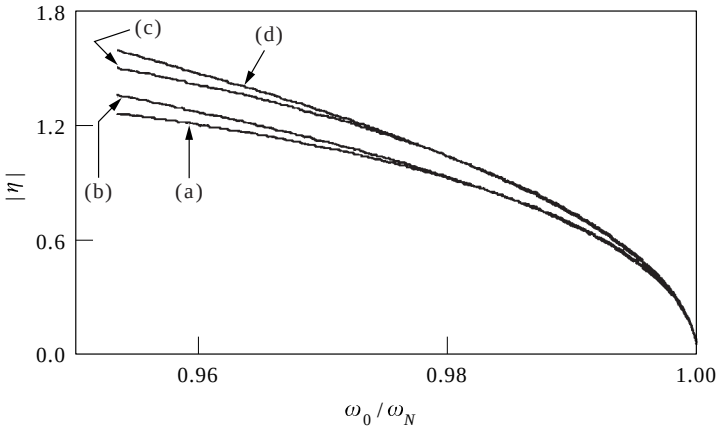

Figure 3. Free undamped vibrations: normalized vertical displacement response $|\eta|$ of the moving cylinder versus the normalized natural frequency ω_0/ω_N. (a) η_{max} (equation 11); (b): η_{max} (equation 13); (c): $|\eta| = \alpha$ (equation 11); (d): $|\eta| = \alpha$ (equation 13).

Approximate solution of this equation, under initial conditions (7) can then be obtained by using the multiple scales method [10] which yields

$$\eta(\tau) = -\left[\frac{\alpha^2}{12} - \frac{\alpha^3}{108}\right] - \left[\alpha - \frac{\alpha^2}{18} + \frac{\alpha^3}{162}\right]\cos\bar{\omega}\tau - \left[\frac{\alpha^2}{36} + \frac{\alpha^3}{324}\right]\cos 2\bar{\omega}\tau + o(\alpha)\cos 4\bar{\omega}\tau, \tag{13}$$

where the contribution of the $\cos 3\bar{\omega}\tau$ term is found to be equal to zero. If the coefficients of the response $\eta(\tau)$ are calculated for $\alpha = -3/2$ (limit of the contact loss), it can be observed that the constant term is small compared with the fundamental (approximately 11%) as well as the first harmonic (less than 4%). We may conclude that non-linearity is low and that the free response spectrum will be dominated by two peaks.

One can also obtain the relationship between natural frequency and amplitude as

$$\bar{\omega}_0 = 1 - \alpha^2/54. \tag{14}$$

Furthermore, the maximum value η_{max} is given by

$$\eta_{max} = \eta(\pi) = \alpha - (\alpha^2/9) + (\alpha^3/81). \tag{15}$$

The approximate analytical results can be validated by comparing them with the previous numerical computation results. A good agreement can be observed in Figure 3 for small and medium amplitudes of $|\eta|$.

3. CONTACT FREE VIBRATIONS: EXPERIMENTAL ANALYSIS

3.1. INTRODUCTION

Figure 1 illustrates the equipment used for the measurements. Two external charge amplifiers connected to an impedance head allow the exciting force produced by the vibration exciter and the acceleration response of the cylinder to be measured. A three-orthogonal-component piezoelectric transducer allows the contact dynamic load transmitted onto the lower plane to be measured and the verticality of the cylinder to be verified. This transducer was rigidly fixed on a rigid and heavy frame (slotting machine's table).

The mass M of the moving cylinder was equal to 10·4 kg. The 100C6 steel planes in contact with the sphere are first straightened, rectified, ground, and then polished to achieve very slight rugosity ($Ra = 0{\cdot}03$ μm). Nineteen different spheres were analyzed to determine the influence of their radius R. These spheres were supplied by a ball bearings maker. They were constructed from 100C6 steel and had a very slight rugosity as well. The selected values ranged from $R = 5$ to 15 mm.

The fine signal analyses were carried out by means of a real-time spectrum analyzer.

3.2. EXPERIMENTAL RESULTS

Figure 4 provides an example of the trend of the normalized contact load $F_T(t)/F_S$ transmitted to the lower plane during free vibrations of the moving cylinder. In this example, the sphere diameter is $2R = 12$ mm and the vertical projection axis of the load is oriented upwards. For every other sphere analyzed, a similar measurement was performed.

The experimental results shown in Figure 4 reveal a single natural frequency: the one-degree-of-freedom model proposed in section 2 is hence experimentally verified. A simple computation shows that for the two-degree-of-freedom system and whatever sphere is used for our tests the value of the second natural frequency is above 4 kHz.

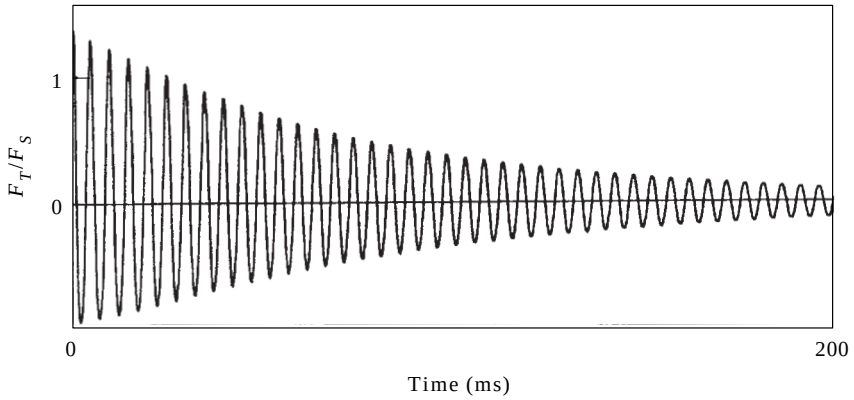

Figure 4. Example of measurements of the normalized normal contact load F_T/F_S versus time during free normal vibrations of the moving cylinder. (Sphere diameter $2R = 12$ mm.)

It has also been verified that the experimental conditions could not invalidate the use of the Hertzian theory. In particular, the computation of the maximum pressure in the contact at the highest dynamic compression forces associated with our tests enabled us to verify that the deformations remain elastic.

From each of the experimental results similar to those in Figure 4, the natural frequency related to the smallest amplitudes was determined and this experimental value was compared with the contact natural frequency ω_N predicted by the theory, equation (6). This comparison showed less than 2·5% difference. This small variation validates the experimental procedure implemented.

The non-linearity of the problem studied is clearly identified in Figure 4 by the asymmetry observed at the highest amplitudes of the free response. This non-linearity also leads to a small variation in the frequency as a function of amplitude. Figure 5 illustrates the changes in the amplitude of the free vibrations (positive peaks) depending on those of the associated frequency. It has been observed in section 2 that the diasymmetry generates two distinct amplitude–frequency curves, depending on whether the maximum or minimum amplitudes are considered. Figure 5 illustrates the theoretical results of the analysis performed in section 2. If η_{max} is the maximum position, then the theoretical

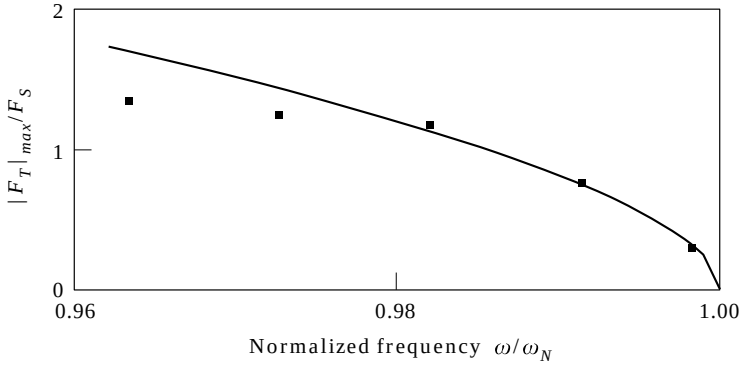

Figure 5. Normalized largest amplitude $|F_T|_{max}/F_S$ of the normal contact load versus the normalized frequency ω/ω_N during free normal vibrations of the moving cylinder. ■, Experiments; ——, theory. (Sphere diameter $2R = 12$ mm.)

analysis provides $|F_T|_{max}$. Figure 5 shows that for frequencies not far from the contact natural frequency, experimental results match the theoretical predictions rather well.

3.3. DAMPING ANALYSIS

3.3.1. *Introduction*

The vibration damping capacity of the Hertzian sphere–plane contact that we are experimentally analyzing and which is excited by a normal harmonic load can have several origins. To the inner damping inherent to the materials used [13, 14], the following phenomena can be added: damping caused by microslidings at the periphery of the contact area [15–17] and generated by the possible existence of a low tangential dynamic load produced by a cylinder verticality defect; damping caused by a fluid pumping mechanism (cyclical discharge and suction applied on the viscous fluid surrounding the contact area); viscous type damping caused by the acoustic radiation of vibrating surfaces (sphere and planes).

From equation (4) the damped free vibrations of the cylinder can be described by the equation

$$\ddot{\eta} + 2\zeta(\eta, \dot{\eta})\dot{\eta} + (1 + \tfrac{2}{3}\eta)^{3/2} = 1, \tag{16}$$

where $\zeta = C'(z, \dot{z})/2M\omega_N$. To analyze the total contact damping, this equation will be numerically solved by testing various laws for $C'(z, \dot{z})$, laws that will be validated or rejected by a comparison with the experimental results (with or without superposition of the experimental and numerical curves describing the free response of the system).

3.3.2. *Numerical simulations and choice of the damping function*

From equation (1), the contact load F_T induced by damped free vibrations of the cylinder on the lower plane of the experimental device can be expressed by

$$F_T = -C'(z, z')\dot{z} - k'(z_0 + z)^{3/2}. \tag{17}$$

In this formula, we have tested the following laws:

$$C'(z, z') = C''(z + z_0)^n, \quad \text{with} \quad n = 0, \quad n = \tfrac{1}{2}, \quad n = 1, \quad n = \tfrac{3}{2}, \quad n = 2, \quad n = \tfrac{5}{2}. \tag{18}$$

C'' is a constant positive coefficient adjusted by dichotomy to minimize the variations between the peaks of the experimental curve and those of the numerically computed curve for each type of law tested.

Figure 6 illustrates an example of the relative variation in the value of each peak of a theoretical curve compared with the associated experimental curve. Note that this variation rarely exceeds 1%. For each law tested, a "global" relative error Δ can be defined. This error can be quantified by introducing the least squares method,

$$\Delta = \sqrt{\frac{1}{N}\sum_{i=1}^{N}\left(\frac{F_{Ti}\,(\text{exp}) - F_{Ti}\,(\text{num})}{F_{Ti}\,(\text{exp})}\right)^2}, \tag{19}$$

which permits calculation of the r.m.s. value of the relative variation. For the first four laws tested, the relative variation ranges around 1% and slightly more for the other laws. No conclusion can then be drawn about the precise analytical form of the total damping law, so the most conventional form, an equivalent viscous type damping ($n = 0$) will now be used. The measured values of the equivalent viscous damping C'' correspond to two symmetrical sphere–plane contacts of the experimental device. For a single sphere–plane contact, values provided should therefore be divided by two.

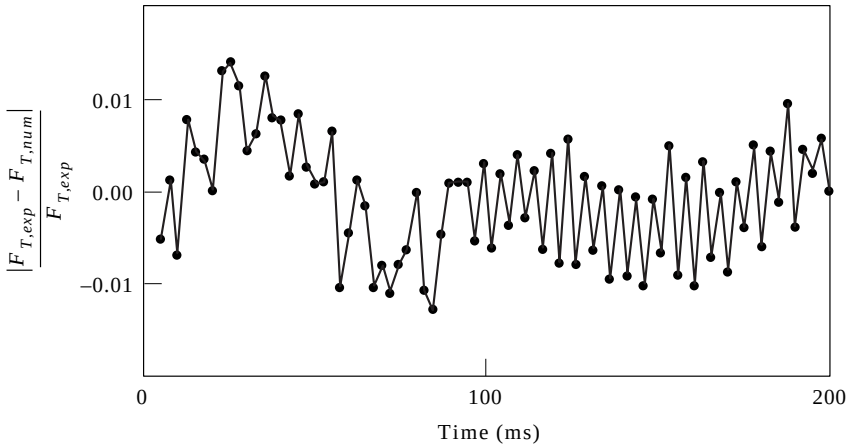

Figure 6. Normalized difference $[F_{T,exp} - F_{T,num}]/F_{T,exp}$ between experimental and computed values of the normal contact load versus time during damped normal free vibrations of the moving cylinder. (Sphere diameter $2R = 12$ mm and viscous damping $C'' = 208$ kg s^{-1}.)

3.3.3. *Influence of sphere radius on contact damping*

The values of the equivalent viscous damping C'' were determined for a variety of sphere diameters from measurements of the free vibrations of the cylinder. From each value obtained, the contact damping ratio (total equivalent viscous damping) was defined by

$$\zeta = C''/2M\omega_N, \tag{20}$$

where ω_N is the theoretical contact natural frequency. The ζ value thus obtained are illustrated in Figure 7. Note that at constant normal load F_s, the equivalent viscous damping ratio slightly increases as a function of the sphere radius R. From these results, function $\zeta = AR^{1/3}$ (with $A =$ constant) was plotted. This law has been observed to represent approximately the damping ratio trend related to sphere radius. Since the normal load F_s is constant in our experiments, the contact area radius of the sphere–plane contact is proportional to $R^{1/3}$. It can then be deduced that at constant normal load, the contact damping ratio is approximately proportional to the radius of the contact area.

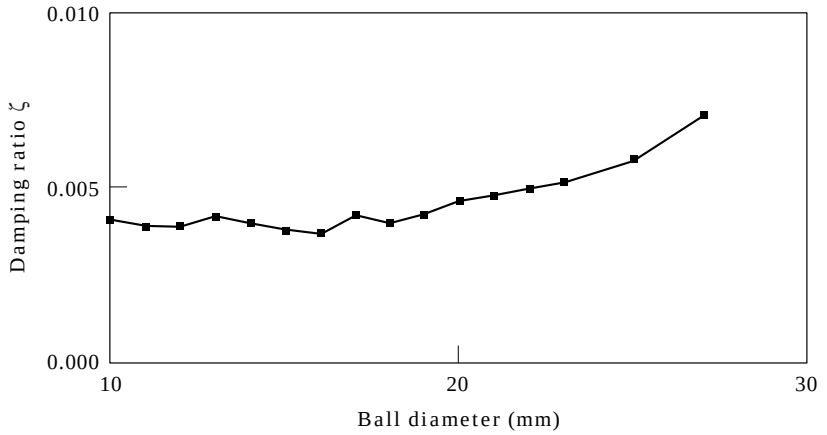

Figure 7. Measurements of the damping factor ζ for dry contacts and several sphere diameters.

At a given normal load, it was also noted that the linearized contact stiffness is inversely proportional to the relative displacement z_0 of both planes. Since z_0 is inversely proportional to $R^{1/3}$, it can be deduced that the measured contact damping ratio is also approximately proportional to the linearized contact stiffness.

3.3.4. *Origins of contact damping*

All spheres analyzed had a low measured contact damping ratio (less than 0·6% for a single sphere–plane contact). In forced vibrations and for a very low level of the harmonic excitation force, the energy dissipated per cycle at contact natural frequency can be evaluated from the relationship [13]

$$W_d = (C''/2)\pi\omega_N \hat{u}^2, \tag{21}$$

where $\hat{u}$ corresponds to the maximum peak amplitude of the displacement response of the cylinder during the cycle. Under the experimental conditions corresponding to a sphere with a diameter of 25·4 mm, W_d approximates 10^{-6} J.

Various physical phenomena could affect the contact damping measured, so the influence of each of them should be known. Regarding the influence of the friction associated with the cyclical microslidings caused at the periphery of the contact area by a verticality defect on the moving cylinder, the following remarks can be made. On the experimental device used, the amplitude of the tangential component of the stress applied on the lower plane was measured by means of a three-component piezoelectric transducer mounted on the lower plane. The verticality of the moving cylinder could then be adjusted so that the tangential load T remained lower than 1/100 of the normal load F_s. By introducing a friction factor μ equal to 1 [17], the $T/\mu F_s$ ratio then approximates 10^{-2}. For this low value, the energy dissipated per cycle in each contact can be given by the simplified formula [16]

$$W_m = (2 - \nu)T^3/36Ga\mu F_s, \tag{22}$$

where ν is the Poisson's ratio and G the shear modulus of the material of the sphere and planes. Under the experimental conditions that correspond to a sphere of diameter $2R = 25{\cdot}4$ mm, the energy dissipated per cycle approximates 10^{-8} J. This contribution to total damping is hence negligible.

For this viscous damping added by acoustic radiation, we know [18] that the acoustic power radiated by a vibrating surface S in harmonic motion can be given by

$$\Pi_{ac} = \rho c S \sigma_{rad}(\omega)\langle\overline{\dot{u}^2}(M, \omega)\rangle_S. \tag{23}$$

In this expression, ρ and c respectively correspond to the density and sound speed associated with the compressible fluid surrounding the surface S (here the air), σ_{rad} is the radiation factor and $\langle\dot{u}^2(M, \omega)\rangle_S$ is the space average of the time average of the r.m.s. velocity response $\dot{u}(M, \omega)$ at a point M on surface S.

In our tests, the largest surfaces that contribute to the radiation are the upper and lower sides of the moving cylinder (cylinder radius = 0·05 m). Both surfaces constitute a rigid unbaffled piston propelled by a uniform velocity $\dot{u}$. Upon assuming that the per unit area radiation resistance σ_{rad} is independent of the point M on the piston surface, the following formula can then be used,

$$R_{rad}(\omega) = \rho c \sigma_{rad}(\omega), \tag{24}$$

and the added viscous damping due to the acoustic radiation of each piston can be expressed as follows

$$C_{ac}(\omega) = SR_{rad}(\omega). \tag{25}$$

The energy dissipated per cycle associated with the acoustic radiation at the contact natural frequency ω_N can finally be expressed as

$$W_d = C_{ac}\,\pi\omega_N\,\hat{u}^2 = \rho c S \sigma_{rad}(\omega_N)\pi\omega_N\,\hat{u}^2. \tag{26}$$

For the radiation factor of an unbaffled piston, there exist no directly usable results so the acoustic radiation software previously developed and used for calculating the noise radiated by a gearbox was used [19]. The radiation factor approximates 0·006. From this value and the experimental data, the energy dissipated by acoustic radiation at contact natural frequency approximates 10^{-10} J. In our tests, this contribution to total contact damping is therefore negligible.

The last source of damping to be considered is the "fluid pumping" phenomenon. There is no model that allows a quantitative evaluation of this dissipation in a sphere–plane contact, so tests were conducted by introducing several viscous fluids on the contact areas before mounting the plane–sphere–plane system. These fluids were water, oil, and several aqueous solutions of glycerine and glycerine. Their dynamic viscosity was approximately located between 10^{-4} and 1·5 Pa s. The new contact damping ratio values thus obtained are given in Figure 8. It clearly appears that the presence of fluid whose dynamic viscosity is high can significantly increase the contact damping. This observation, linked to the fact that the measured contact natural frequency is not significantly modified by the presence of a viscous fluid, indicates that the fluid pumping phenomenon significantly contributes to total contact damping if the dynamic viscosity of the fluid surrounding the contact is high.

Let us now assume that the equivalent viscous damping ratio caused by the fluid pumping phenomenon is proportional to the dynamic viscosity μ of the fluid surrounding the contact, which is to say

$$\xi_{FP} \approx \beta\mu \qquad \text{where} \qquad \beta = \text{constant}. \tag{27}$$

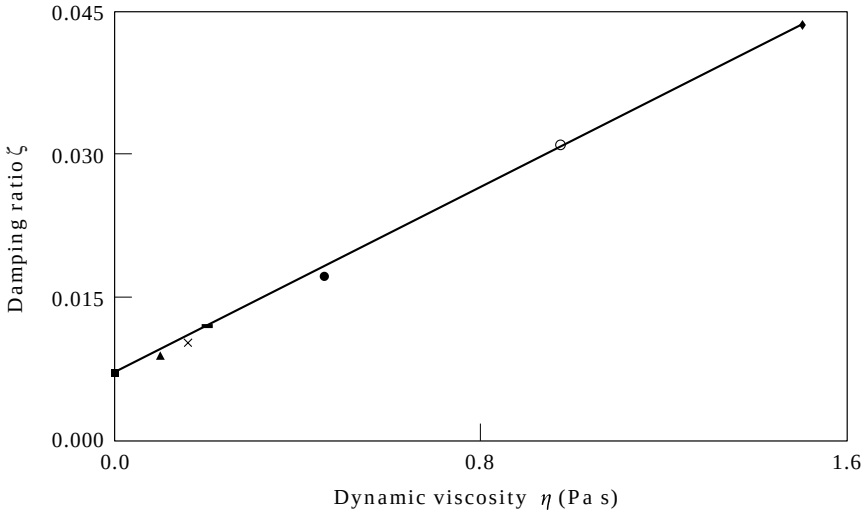

Figure 8. Measurements of the damping factor ξ for lubricated contacts (water, oil, aqueous solutions of glycerine, and glycerine) and for a sphere diameter $2R = 25{\cdot}4$ mm.

The total damping ratio can then be expressed as

$$\zeta = \zeta_{int} + \beta\mu, \tag{28}$$

where ζ_{int} is the damping factor due to internal damping inherent to the materials used for the sphere and the planes.

The results shown in Figure 8 are in good agreement with the proposed law (28).

4. FORCED CONTACT VIBRATIONS: EXPERIMENTAL ANALYSIS

4.1. INTRODUCTION

After analyzing the free vibrations of the elastic plane–sphere–plane system, a second set of experimental investigations were performed to analyze the specification of the non-linear forced vibrations of this system when it is excited by a normal dynamic load equal to the sum of a static load F_S and a purely harmonic load of frequency ω and amplitude F_e which is sufficiently low to avoid the occurrence of contact losses between sphere and planes.

During our investigations, we focused on the analysis of the dynamic contact load F_T transmitted by the sphere onto the lower plane. The understanding of this load is of the utmost importance for the analysis of the higher overloads applied on contacts and hence for the prediction of the life duration and vibroacoustic response of mechanisms.

For the one-degree-of-freedom elastic model associated with our plane–sphere–plane system, the dimensionless equation governing the cylinder's displacement in forced mode can be expressed as

$$\ddot{\eta} + 2\zeta\dot{\eta} + (1 + \tfrac{2}{3}\eta)^{3/2} = 1 + \sigma\cos\bar{\omega}\tau, \tag{29}$$

where $\zeta = C''/2M\omega_N$. In this equation, and in agreement with the conclusions in section 3, the existence of a viscous contact damping C'' is assumed.

4.2. EXPERIMENTAL CONDITIONS

The experimental conditions are the same as those described in section 3. The normal harmonic force of amplitude F_e and frequency ω is applied on the upper face of the moving cylinder by means of a vibration exciter and it is measured by means of an impedance head placed between the vibration exciter and cylinder (see Figure 1). An external charge amplifier also allows measurement of the cylinder's acceleration or velocity.

The three orthogonal components piezoelectrical transducer is fixed onto the lower plane (see Figure 1) and allows (1) measurement of the contact load F_T, (2) adjustment of cylinder verticality, and (3) checking of the absence of contact losses between ball and planes.

The experimental data at a fixed excitation level F_e and variable excitation frequency described the cylinder acceleration (or velocity) and contact load F_T transmitted onto the lower plane during the cylinder's forced response. The non-linear resonance curve plotting provided the trend of the r.m.s. value of these responses and also their frequency contents.

Among the numerous measurements made, those obtained with a sphere of diameter $2R = 18$ mm are described here as an example. The measurements relate to the specification of contact load F_T. The other cylinder acceleration (or velocity) response data offer similar general specification.

During frequency scans performed for a very small level of exciting force and for various sphere diameters, it could be verified that within the 20–3000 Hz frequency range, there was no other significant resonance phenomenon than that of our elastic plane–sphere–plane system. It will be observed that, considering the following data, the phenomenon

is centred around contact natural frequency ω_N and over a small frequency span around this natural frequency.

4.3. NON-LINEAR RESONANCE

Figure 9 illustrates the principal non-linear resonance phenomenon observed on the contact load during a scan of increasing frequency and during a scan of decreasing frequency at an amplitude of excitation force F_e equal to 0·018 times the static load F_S. A dynamic behaviour associated with a softening stiffness can be recognized since the scan of decreasing frequency is associated with the highest dynamic response. Just before the corresponding jump, the r.m.s. value of the contact load reaches a high amplitude nearing static load F_S. This result indicates that forced contact vibrations can generate instantaneous high overloads on contacts. The frequencies associated with both jump phenomena are rather similar because non-linearity is low. The dynamic amplification phenomenon due to non-linear resonance is significant only over a small frequency span (between 0·95 and 1·05 ω_N). Figure 9 also shows the trace of the tangential force caused by the verticality defect on the moving cylinder. Notice that this tangential component is very low compared with the normal force. For the very small levels of exciting force used to study the principal non-linear resonance of our system we have not observed secondary non-linear resonances [20].

Figures 10 and 11 respectively describe the periodic time trend of the contact load and the spectrum of this function at harmonic excitation frequency equal to 0·97 times contact natural frequency, which is to say just before the jump observed during a scan at decreasing frequency, and hence at a high amplitude of the vibration response. The dissymetry of the plotting shown in Figure 10 illustrates the small non-linearity of the dynamic response. In Figure 11, the spectrum of this response shows that three harmonics of the excitation frequency are present, but only the first has a significant amplitude (about 10% of that of the fundamental). It can then be concluded that, in agreement with the conclusions of

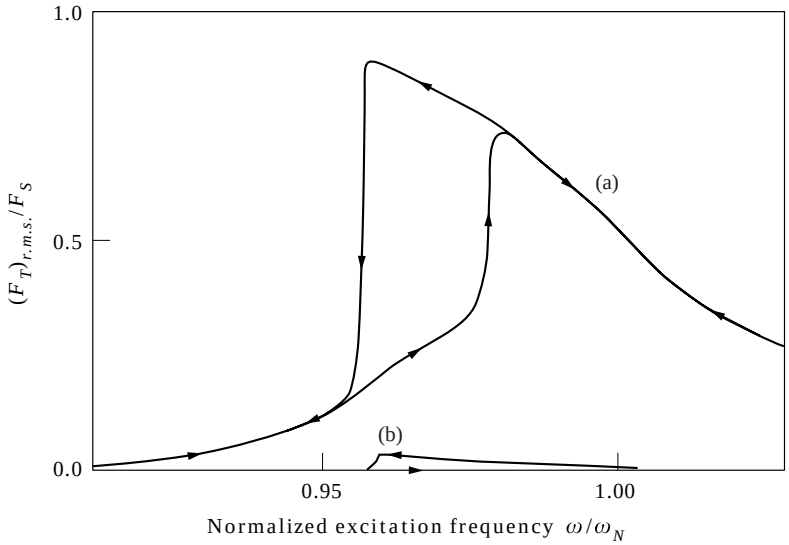

Figure 9. Measurements of the normalized r.m.s. value $(F_T)_{r.m.s.}/F_S$ of the contact load versus the normalized excitation frequency ω/ω_N for a harmonic excitation force $(F_e)_{r.m.s.}/F_S = 0{\cdot}018$ and a sphere diameter $2R = 18$ mm. (a) Normal component; (b) ten times the tangential component.

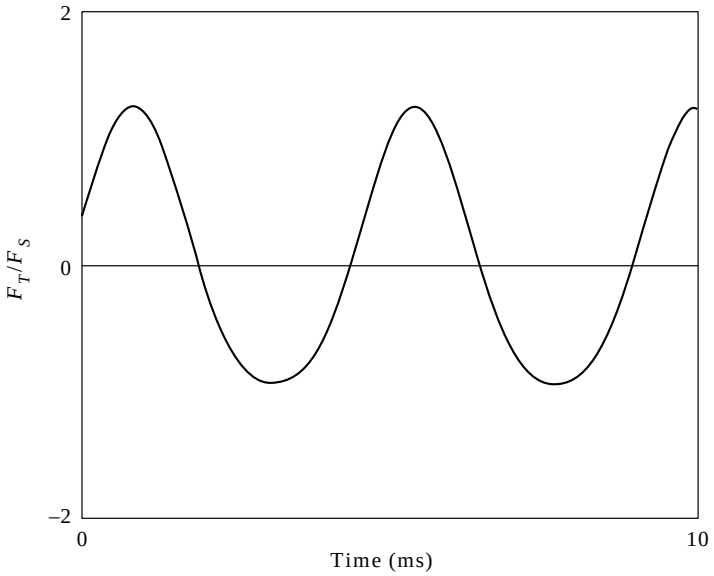

Figure 10. Measurements of the normalized contact load F_T/F_S versus time for a normalized excitation frequency $\omega/\omega_N = 0{\cdot}965$ during a scan at decreasing frequency. Sphere diameter $2R = 18$ mm, normalized excitation force $(F_e)_{r.m.s.}/F_S = 0{\cdot}018$.

the theoretical analysis in section 2, the dynamic spectrum which characterizes the non-linear resonance is a two-peak spectrum.

Figure 12 shows the trend of the r.m.s. value of the contact load associated with each of its two harmonic components. The jump phenomena can be observed on both components.

Figure 13 illustrates the effect of amplitude F_e of the excitation force on the non-linear resonance phenomenon. Note that for the system analyzed, jump phenomena can be

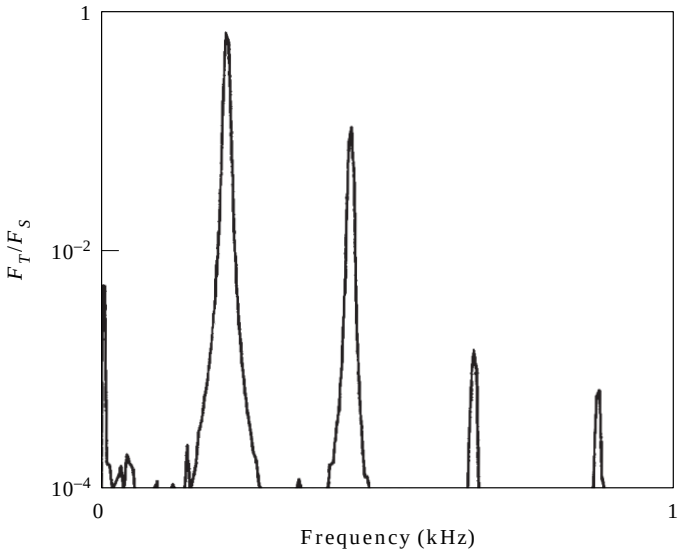

Figure 11. Spectrum of the normalized contact load F_T/F_S shown in Figure 9.

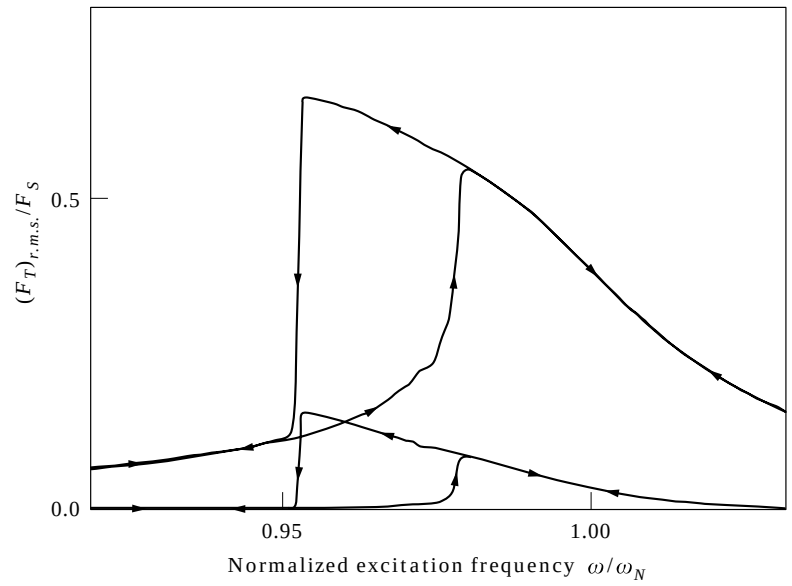

Figure 12. Measurements of the normalized r.m.s. value $(F_T)_{r.m.s.}/F_S$ of the contact load versus the normalized excitation frequency ω/ω_N for (a) the excitation frequency and (b) the first harmonic of the excitation frequency. (Sphere diameter $2R = 18$ mm and harmonic excitation force $(F_e)_{r.m.s.}/F_S = 0{\cdot}018$.)

observed over a very small frequency F_e span only. In fact, when the amplitude F_e is very low, the slight non-linearity of the system stiffness leads to a linear resonance curve, whereas if the amplitude F_e exceeds a specific level (a level that is relatively small under

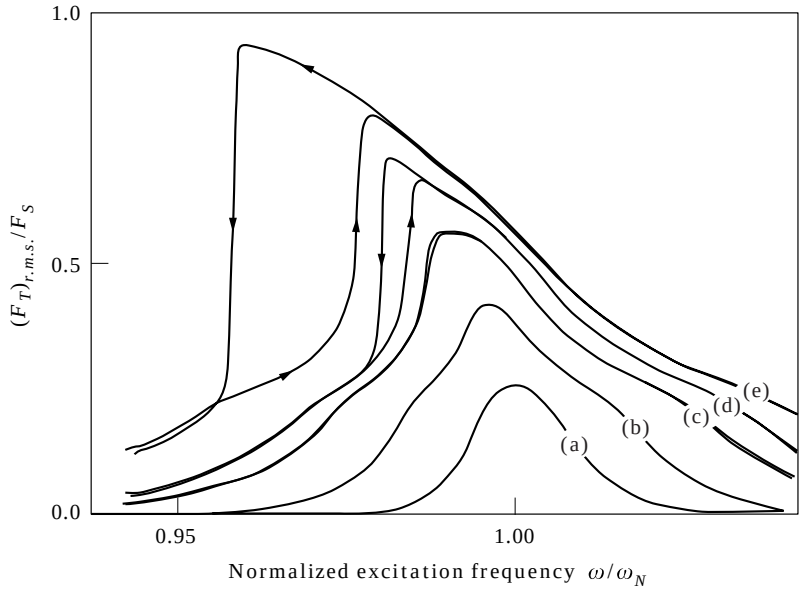

Figure 13. Measurements of the normalized r.m.s. value of the normal contact load excitation frequency, for several values of the normalized r.m.s. excitation force $(F_e)_{r.m.s.}/F_S$: (a) 5×10^{-3}; (b) $7{\cdot}8 \times 10^{-3}$; (c) $1{\cdot}5 \times 10^{-2}$; (d) $1{\cdot}7 \times 10^{-2}$; (e) $1{\cdot}85 \times 10^{-2}$. (Sphere diameter $2R = 18$ mm.)

our experimental conditions), contact losses occur between sphere and planes. A series of impacts governs the cylinder's dynamic behaviour.

5. CONCLUSIONS

An efficient device has been built and used to study the non-linear vibrations of a sphere–plane contact excited by a normal load equal to the sum of a static load and a harmonic load. Numerous experimental and numerical investigations have provided the following main results.

For free contact vibrations, it has been observed that: the measured contact natural frequency is in very good agreement with the theory; the damping contact in a dry contact is small and can be well described by a viscous damping; this equivalent viscous damping can result from several sources; in a dry contact, the total damping is mainly due to the damping materials; in a lubricated contact, a fluid-pumping type mechanism can add a noticeable amount of damping to the existing damping materials.

For forced contact vibrations induced by a small harmonic load added to the normal static load, it has been shown that: the non-linear resonance of a sphere–plane type contact is that of a softening system; the largest amplitude of the dynamic contact load is obtained just before the jump observed during a scan of decreasing frequency and can reach values twice as large as the static load for a very small amplitude of the harmonic load (about 1% of the static load); when the amplitude of the harmonic load is slightly increased, losses of contact appear and a succession of impacts is observed; these impacts, which can arise in mechanisms exhibiting clearances, can therefore induce high levels of vibration, noise and dynamic loading of contacts.

ACKNOWLEDGMENTS

The authors wish to express their gratitude to Dr J. Perret-Liaudet for many illuminating discussions on numerical aspects in non-linear vibrations. This work was supported by the Groupement de Recherche Vibroacoustique of the French Centre National de la Recherche Scientifique and by Renault V.I. this support is gratefully acknowledged.

REFERENCES

1. H. Hertz 1882 *Journal reine und angewandte Mathematik* **92**, 156–171. Über die Berührung fester elastischer Körper.
2. S. P. Timoshenko and J. N. Goodier 1951 *Theory of Elasticity*. New York: McGraw-Hill.
3. K. L. Johnson 1985 *Contact Mechanics*. Cambridge University Press.
4. R. D. Mindlin 1949 *ASME Journal of Applied Mechanics* **16**, 259–268. Compliance of elastic bodies in contact.
5. D. B. Welbourn 1979 *Proceedings of the Institution of Mechanical Engineers. Conference of Noise and Vibrations of Engines and Transmissions—Cranfield* **C117/79**, 9–29. Fundamental knowledge of gear noise—a survey.
6. R. M. Carson and K. L. Johnson 1971 *Wear* **17**, 59–72. Surface corrugations spontaneously generated in a rolling contact disc machine.
7. P. Ranganath Nayak 1972 *Journal of Sound and Vibration* **22**, 297–322. Contact vibrations.
8. H. P. Hess, A. Soom and C. H. Kim 1991 *ASME Journal of Tribology* **113**, 80–86. Normal vibrations and friction under harmonic loads, Part I: Hertzian contacts.
9. H. P. Hess, A. Soom and C. H. Kim 1992 *Journal of Sound and Vibration* **153**, 491–508. Normal vibrations and friction at a Hertzian contact under random excitation: theory and experiments.
10. A. H. Nayfeh and D. T. Mook 1979 *Nonlinear Oscillations*. New York: John Wiley.

11. R. E. Mickens 1981 *An Introduction to Non-Linear Oscillations*. Cambridge University Press.
12. C. W. Bert and J. D. Stricklin 1988 *Journal of Sound and Vibration* **127**, 221–229. Comparative evaluation of six different numerical integration methods for non-linear dynamic systems.
13. L. Cremer and M. Heckl 1973 *Structure-Borne Sound*. Berlin: Springer-Verlag. Section III: Damping. See pp. 205–209.
14. A. D. Nashif, D. I. G. Jones and J. P. Henderson 1985 *Vibration Damping*. New York: John Wiley.
15. K. L. Johnson 1955 *Proceedings of the Royal Society of London A* **230**, 531–548. Surface interaction between two elastically loaded bodies under tangential forces.
16. J. P. Mindlin, W. P. Mason, J. F. Osmer and H. Deresiewicz 1952 *Proceedings of the First National Congress on Applied Mechanics*, 203–208. Effects of an oscillating tangential force on the contact surfaces of elastic spheres.
17. A. Tonck, J. Sabot and J. M. Georges 1983 *ASME Journal of Lubrification Technology* **11**, 1–8. Microdisplacements between two elastic bodies separated by a thin film of polystyrene.
18. P. M. Morse and K. U. Ingard 1968 *Theoretical Acoustics*. New York: McGraw-Hill.
19. P. Ducret and J. Sabot 1998 *Acustica United with Acta Acustica* **83**, 97–107. Calcul du bruit rayonné par les carters des transmissions à engrenages: méthode et applications.
20. J. Perret-Liaudet 1997 *Comptes Rendus Académie des Sciences Paris* **t.325** Série II b, 443–448. Résonance sous-harmonique d'ordre deux dans un contact sphère–plan.